Cell Reports
Article

Depletion of Cognate Charged Transfer RNA Causes Translational Frameshifting within the Expanded CAG Stretch in Huntingtin

Hannah Girstmair,[1,3] Paul Saffert,[1,3] Sascha Rode,[1] Andreas Czech,[1] Gudrun Holland,[2] Norbert Bannert,[2] and Zoya Ignatova[1,*]
[1]Department of Biochemistry and Biology, University of Potsdam, Karl-Liebknecht-Str. 24-25, 14476 Potsdam, Germany
[2]Robert Koch Institute, Nordufer 20, 13353 Berlin, Germany
[3]These authors contributed equally to this work
*Correspondence: ignatova@uni-potsdam.de
http://dx.doi.org/10.1016/j.celrep.2012.12.019

SUMMARY

Huntington disease (HD), a dominantly inherited neurodegenerative disorder caused by the expansion of a CAG-encoded polyglutamine (polyQ) repeat in huntingtin (Htt), displays a highly heterogeneous etiopathology and disease onset. Here, we show that the translation of expanded CAG repeats in mutant Htt exon 1 leads to a depletion of charged glutaminyl-transfer RNA (tRNA)$^{Gln\text{-}CUG}$ that pairs exclusively to the CAG codon. This results in translational frameshifting and the generation of various transframe-encoded species that differently modulate the conformational switch to nucleate fibrillization of the parental polyQ protein. Intriguingly, the frameshifting frequency varies strongly among different cell lines and is higher in cells with intrinsically lower concentrations of tRNA$^{Gln\text{-}CUG}$. The concentration of tRNA$^{Gln\text{-}CUG}$ also differs among different brain areas in the mouse. We propose that translational frameshifting may act as a significant disease modifier that contributes to the cell-selective neurotoxicity and disease course heterogeneity of HD on both cellular and individual levels.

INTRODUCTION

Expansion of the polyglutamine (polyQ) repeat beyond a critical threshold length causes progressive neuronal dysfunction in the group of dominantly inherited neurodegenerative disorders known as CAG- or polyQ-repeat diseases, including Huntington disease (HD) and several types of spinocerebellar ataxia (SCA) (Orr and Zoghbi, 2007). Strikingly, although the disease-related polyQ proteins are widely expressed in various tissues, each one exhibits a cell-specific pattern of toxicity and triggers the degeneration of specific neuronal populations. Thus, the expansion of the polyQ stretch alone cannot explain the diversity of cell-selective neurotoxicity in polyQ diseases.

Tissue-specific variations in the length of polyQ may contribute to the cell-selective pathogenesis. Within one individual, the CAG stretch is several repeats longer in brain areas than in other tissues (Gonitel et al., 2008; Kennedy et al., 2003). Moreover, the aggregation of the polyQ proteins can be profoundly influenced by sequences flanking the polyQ stretch (Andresen et al., 2007; Tam et al., 2009; Thakur et al., 2009), the cellular environment (Gidalevitz et al., 2006), and cell-type-specific processing or localization of the mutant protein (Toneff et al., 2002). Variations in the flanking sequences may modulate the threshold length of aggregation of each polyQ protein. Huntingtin (Htt) is pathogenic when the length of polyQ exceeds ~35 glutamines, whereas ataxin-3 is pathogenic at ~50 glutamines (Andresen et al., 2007). Intriguingly, the clinical course and onset of each polyQ disease can vary significantly even among patients with identical polyQ-repeat lengths (Brinkman et al., 1997).

The genetic information in neurons is not stable; it is subject to modifications and frameshifting (van Leeuwen et al., 1998) through yet-unknown mechanisms. Postmortem analyses of HD-affected brain tissues revealed traces of polyalanine (polyA) or polyserine (polyS) proteins within the polyQ aggregates (Davies and Rubinsztein, 2006). Whether these species result from a shift in the Gln-encoding CAG frame to an Ala-encoding −1 GCA frame or a Ser-encoding +1 AGC frame is still unclear. In aggregates of expanded ataxin-8, proteins in polyQ, polyA, and polyS frames have been found that result from repeat-associated, non-AUG-initiated translation (Zu et al., 2011). A −1 translational frameshift was observed by expression of the mutant *SCA3* gene encoding ataxin-3 with an expanded polyQ stretch in a cellular model (Toulouse et al., 2005). Homopolymeric alanine expansions are also linked to some aggregation pathologies, most of which are not associated with a neurodegenerative phenotype; only the polyA expansion in the *PABPN1* gene product, which has been implicated in oculopharyngeal muscular dystrophy, displays some pathological features similar to those of the polyQ diseases (Amiel et al., 2004). Compared with polyQ stretches, much shorter expansions of polyA can confer cellular dysfunction and toxicity (Amiel et al., 2004). Translational frameshifting may play a crucial role in the pathogenesis of polyQ diseases. However, the precise effect of the frameshifted species on polyQ aggregation and toxicity remains a fundamentally unresolved issue that raises several important questions: What triggers the frameshifting? What is the frequency of frameshifting? Does it depend on the length of the

CAG repeat encoding the polyQ stretch? Is it cell type specific? How do the frameshifted species modulate the aggregation of the remaining pool of proteins with expanded polyQ tracts?

To address these questions, we performed a systematic analysis of the frequency of frameshifting within the CAG repeat of Htt exon 1 in two different cell lines: neuroblastoma N2a cells and epithelial HeLa cells. We observed predominantly −1 frameshifting, which occurred with an equal stochastic probability at any CAG codon within the expanded CAG repeat. A cohort of frameshifted proteins with different hybrid polyQ/A stretches was formed, as confirmed by mass spectrometry (MS) analysis. Frameshifted polyQ/A proteins caused marked changes in the aggregation of Htt exon 1 with expanded polyQ both in vivo and in vitro. This effect strongly depended on the Q:A ratio and on a complex crosstalk between the polyA segment and N17, both of which have an intrinsic propensity to sample helical conformations. We found that depletion of charged glutaminyl-transfer RNA (tRNA)$^{Gln\text{-}CUG}$ pairing to the CAG codon was the main cause of −1 frameshifting. This was enhanced by a decrease of the tRNA$^{Gln\text{-}CUG}$ level mediated by small interfering RNA (siRNA). Intriguingly, the neuroblastoma N2a cells had a lower amount of tRNA$^{Gln\text{-}CUG}$ than the epithelial HeLa cell line, which correlates with the higher frameshifting frequency observed in the N2a cells. We further found that the tRNA$^{Gln\text{-}CUG}$ concentration was lower in the striatal and hippocampal tissues of mice than in the cortical and cerebellar regions. Our results suggest that frameshifting within expanded CAG stretches may contribute to the heterogeneity in the course and onset of HD on both cellular and individual levels.

RESULTS

Translational Frameshifting within the CAG Repeat Generates Hybrid PolyQ/A Proteins

To monitor frameshifting within the CAG stretch, we fused in a −1 reading frame the yellow fluorescent protein (YFP) to Htt exon 1 with 51Q (Htt51Q(−1)YFP; Figure 1A) and transfected this reporter construct in neuroblastoma N2a cells stably expressing fusions of Htt exon 1 and cyan fluorescent protein (Htt exon 1-CFP) with different polyQ expansions (Yamamoto et al., 2006). The number of cells with frameshifted, YFP-positive species increased in parallel with the polyQ-length increase of chromosomally expressed HttQ-CFP proteins (Figures 1B and 1C). Note that +1 frameshifting was rarely detected in our experiments. −1 Frameshifting is not specific to the neuroblastoma N2a cell line: in HeLa cells we also detected a large number of YFP-positive cells in cells chromosomally expressing HttQ-CFP proteins with longer polyQ expansions (Figure S1A). Notably, we observed YFP-fluorescent species of ectopically expressed Htt51Q(−1)YFP reporter only in the control N2a cells but not in the HeLa cells (Figures 1B, 1C, and S1A). In general, the frequency of YFP-positive cells was higher in the N2a cells than in the equivalent HeLa cell lines (Figures 1C and S1A). This cannot be attributed to differences in messenger RNA (mRNA) expression levels, because the Htt51Q(−1)YFP reporter or chromosomally encoded HttQ-CFP proteins were expressed at similar levels in all cells (Figures S1B, S1C, S1E, and S1F). Moreover, variation in the transfection efficiency is not likely to have caused the effect, because similar transfection efficiencies were achieved among the HeLa and N2a cell lines (see the legends to Figures 1C and S1A).

Next, we sought to identify the positions at which frameshifting occurs by analyzing the frameshifted proteins formed in N2a/Htt103Q-CFP cells transfected with the Htt51Q(−1)YFP reporter. We used hemagglutinin (HA) antibodies that recognize the N-terminal HA tag of Htt51Q(−1)YFP to detect frameshifted proteins with a canonical ATG start codon. Together with the nonframeshifted Htt51Q protein, we observed a smear with a faint laddering pattern toward higher molecular masses (Figure 1D). MALDI-TOF-MS analysis revealed that the multiple HA-positive bands (Figure 1D) corresponded to HttQ/A-YFP proteins with Q:A ratios ranging from Q1:A49 to Q48:A2 (Figure 1E). This finding strongly indicates that a −1 frameshift can occur stochastically in position, at any CAG codon within the CAS stretch, and its frequency is modulated by the amount of CAG codons that have been translated simultaneously and by the cellular background.

Depletion of Aminoacyl-tRNA$^{Gln\text{-}CUG}$ Causes a Translational Frameshift

The observed dependence of the frequency of −1 frameshifting on the CAG length raised an intriguing question as to whether there is a link between frameshifting and the availability of the tRNA$^{Gln\text{-}CUG}$ that pairs exclusively to the CAG codon. Intriguingly, we did not observe any differences in the concentration of total tRNA$^{Gln\text{-}CUG}$ in N2a or HeLa cells coexpressing Htt51Q(−1)YFP and different HttQ-CFP proteins (Figures 2A and S1H), implying that the host cell did not upregulate the transcription of tRNA$^{Gln\text{-}CUG}$ to meet the increased demand. We next measured the amount of aminoacylated tRNA$^{Gln\text{-}CUG}$, because only a charged tRNA can enter a translation cycle. We isolated the total tRNA under acidic conditions to preserve the aminoacyl groups and quantified it by northern blot. The polyQ repeat of the Htt51Q(−1)YFP reporter is encoded solely by the CAG codon, whereas the polyQ stretches of the chromosomally integrated Htt25Q-CFP, Htt65Q-CFP, and Htt103Q-CFP are composed by alternating the two glutamine codons, CAA and CAG (Yamamoto et al., 2006), which are read by tRNA$^{Gln\text{-}UUG}$ and tRNA$^{Gln\text{-}CUG}$, respectively. Thus, translation of one copy of the ectopically expressed Htt51Q(−1)YFP reporter together with one copy of chromosomally encoded Htt25Q-CFP, Htt65Q-CFP, or Htt103Q-CFP would require 64, 84, or 103 copies, respectively, of glutaminyl-tRNA$^{Gln\text{-}CUG}$. Intriguingly, the amount of glutaminyl-tRNA$^{Gln\text{-}CUG}$ dropped significantly in parallel with the CAG-length increase of the chromosomally expressed HttQ-CFP proteins in the host cell (Figure 2A).

To confirm that the observed differences in frameshifting were modulated by tRNA$^{Gln\text{-}CUG}$, we upregulated or downregulated the tRNA$^{Gln\text{-}CUG}$ level and analyzed the frameshifting frequency in N2a cells expressing the Htt51Q(−1)YFP reporter. A partial decrease of tRNA$^{Gln\text{-}CUG}$ using a specific siRNA probe directed against tRNA$^{Gln\text{-}CUG}$ (Figure S2) increased the number of YFP-positive N2a cells compared with the control (Figure 2B). This effect was specific, because a siRNA probe targeting tRNA$^{Thr\text{-}AGU}$, which is unrelated to the translation of the CAG repeat, had no effect (Figure 2B). Note that tRNA$^{Gln\text{-}CUG}$ can

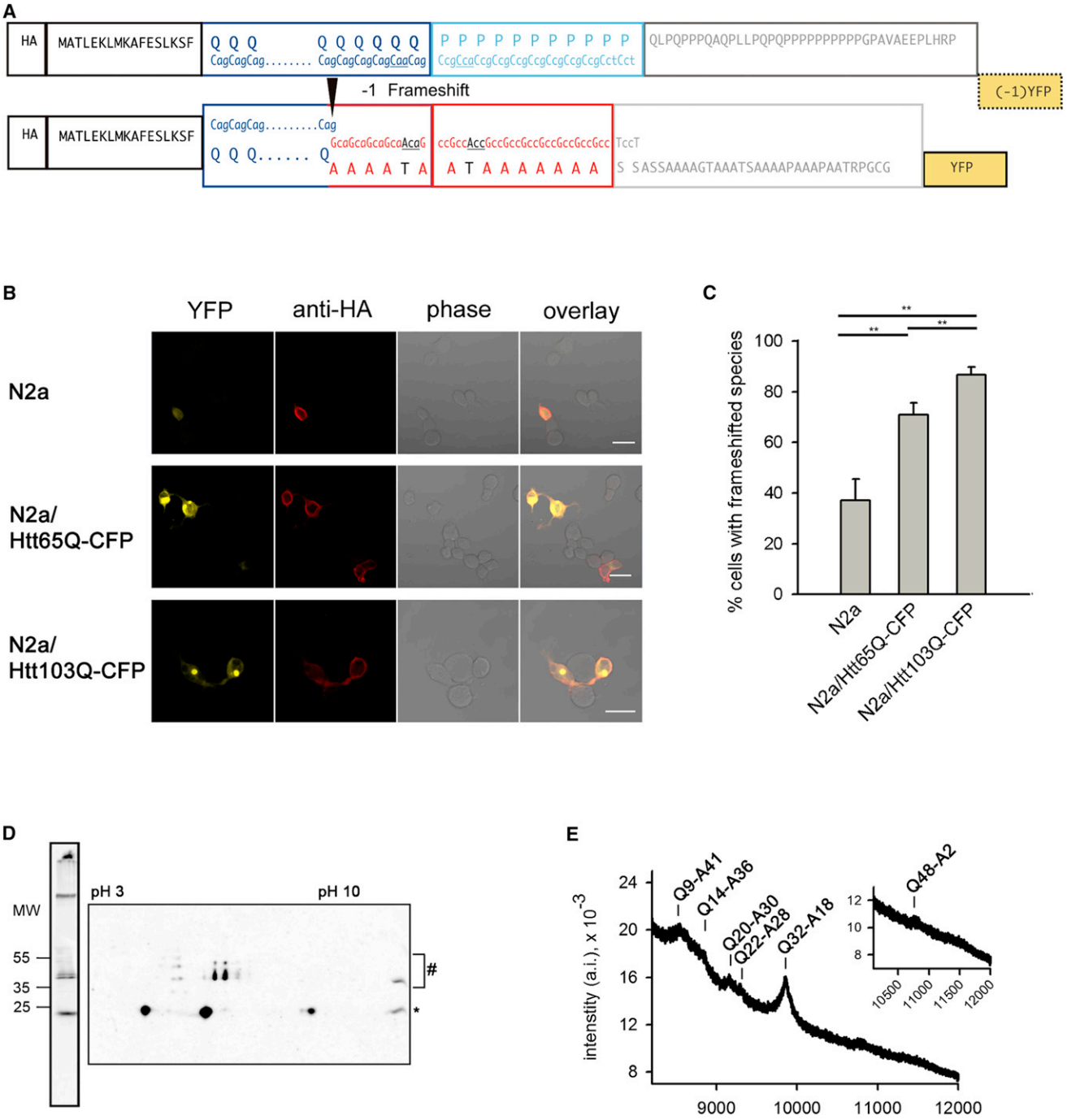

Figure 1. Frameshifting within the Homopolymeric CAG Repeat

(A) Schematic representation of −1 frameshifting within the CAG stretch (dark blue) of Htt51Q(−1)YFP to a GCA-reading frame encoding Ala (red). The first polyP (light blue) is changed to polyA, and the second polyP and the C-terminal Q/P-rich segment are changed to an Ala-rich region. The penultimate Gln residue of the polyQ and the second Pro of the polyP are encoded by their synonymous CAA and CCA codons (black, underlined), thus interrupting the Ala repeat with two Thr residues. The first nucleotide of each triplet is capitalized to highlight each reading frame.

(B) N2a, N2a/Htt65Q-CFP, and N2a/Htt103Q-CFP cells were transiently transfected with the Htt51Q(−1)YFP reporter and visualized by fluorescence (YFP) and phase contrast (phase) microscopy after 24 hr. Htt51Q and Htt51QYFP expression was monitored by immunostaining of the N-terminal HA tag. Scale bar, 10 μm.

(C) The percentage of cells containing YFP-positive, frameshifted aggregates from the total amount of cells transfected with Htt51Q(−1)YFP (i.e., HA-positive). Transfection efficiency was 45.7% ± 4.1% for N2a, 44.2% ± 6.3% for N2a/Htt65Q-CFP, and 46.1% ± 4.8% for N2a/Htt103Q-CFP cells. The values are expressed as the means of five independent experiments ± SEM. **$p < 0.01$.

(legend continued on next page)

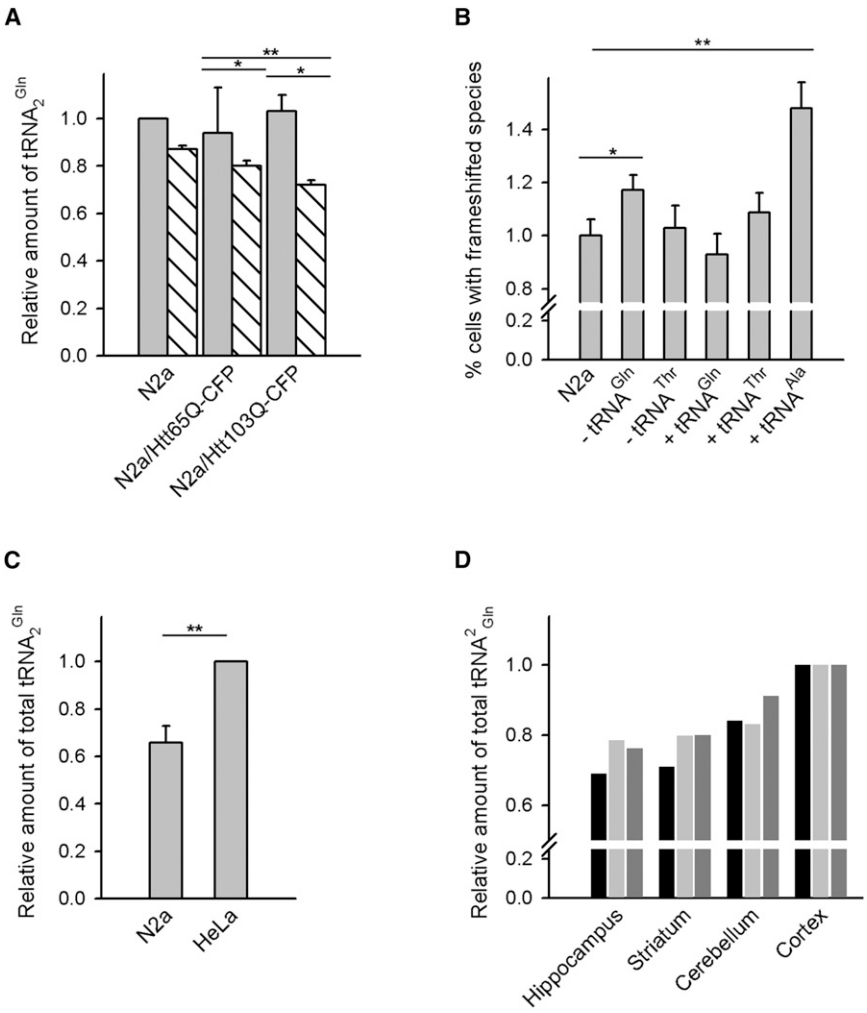

Figure 2. Glutaminyl-tRNA$^{Gln\text{-}CUG}$ Concentration Decreases in a CAG-Length-Dependent Manner and Differs in Cells and Tissues

(A) Total (gray) and aminoacylated-tRNA$^{Gln\text{-}CUG}$ (white) levels quantified from northern blots. The intensity of total tRNA$^{Gln\text{-}CUG}$ of each sample is normalized to the intensity of tRNA$^{Gln\text{-}CUG}$ of the control N2a cells. Glutaminyl-tRNA$^{Gln\text{-}CUG}$ is determined as a fraction of the total tRNA$^{Gln\text{-}CUG}$ in each sample. Values are the mean ± SD of three independent experiments. Equal amounts of the total RNA were loaded onto the northern blots. *$p < 0.05$, **$p < 0.01$.

(B) Changes in the tRNA$^{Gln\text{-}CUG}$ level alter the frameshifting frequency in cells expressing Htt51(−1)YFP. tRNA$^{Gln\text{-}CUG}$ was silenced with siRNA complementary to nucleotides 21–39 (−tRNA^{Gln}) or upregulated by transfection with in vitro transcribed tRNA$^{Gln\text{-}CUG}$ (+tRNA^{Gln}). Downregulation (−tRNA^{Thr}) or upregulation (+tRNA^{Thr}) of tRNA$^{Thr\text{-}AGU}$, which is unrelated to translation of the CAG stretch, had no effect. The upregulation of tRNA$^{Ala\text{-}UGC}$ (+tRNA^{Ala}) had a tremendous effect on the frequency of frameshifting. In each experiment, cells were cultured for 24 hr after the tRNA-level manipulations. The frameshifting is represented as the percentage of cells (±SEM) containing YFP-positive aggregates in the total population of cells transfected with Htt51Q(−1)YFP (i.e., HA-positive) and compared with the control cells (N2a) for which the percentage of frameshifted cells was set as one. *$p < 0.05$, **$p < 0.01$.

(C) Northern blot analysis of the total tRNA$^{Gln\text{-}CUG}$ isolated from N2a and HeLa cells. Equal amounts of total RNA were loaded onto the gel, and blots were hybridized with probes against tRNA$^{Gln\text{-}CUG}$ and 5 s ribosomal RNA (rRNA). The intensity of the tRNA$^{Gln\text{-}CUG}$ band is related to the intensity of 5 s rRNA and the values are shown as the mean ± SD of three independent experiments. The values of HeLa cells were arbitrarily set as one. **$p < 0.01$.

(D) Total tRNA$^{Gln\text{-}CUG}$ concentration in various brain regions of three C57B16 mice (black, mouse 1; light gray, mouse 2; dark gray, mouse 3) at 8 weeks of age. For each mouse, the tRNA$^{Gln\text{-}CUG}$ concentration in the cortex was arbitrarily set as one.

See also Figure S2.

only be partially downregulated (here by ~40%; Figure S2) because a complete knockdown would perturb the global translation and vitality of the cell. In contrast to the pronounced effect of the tRNA$^{Gln\text{-}CUG}$ downregulation, the tRNA$^{Gln\text{-}CUG}$ upregulation (Figure S2) by transfecting in vitro transcribed tRNA$^{Gln\text{-}CUG}$ (Geslain and Pan, 2010) had no effect: the frameshifting frequency was similar to that observed in both the control N2a cells and cells with upregulated control tRNA$^{Thr\text{-}AGU}$ (Figure 2B). Conversely, the upregulation of tRNA$^{Ala\text{-}UGC}$, which pairs to the GCA codon in the −1 transframe, dramatically increased the frameshifting frequency (Figure 2B). Atkins et al. (1979) observed an analogous effect in a study of the MS2 virus coat gene, in which they detected enhanced frameshifting by adding tRNA cognate to the codon in the −1 frame. Aminoacylation is a rate-limiting step in eukaryotes (Zhang et al., 2010). Thus, an increase in tRNA concentration would result in an enhanced level of aminoacylated tRNA only if the natural concentration of this tRNA in the cell were below or nearly equal to the K_m value of the corresponding aminoacyl-tRNA synthetase, i.e., an effect would be observed mostly for low-abundance tRNAs. In eukaryotic cells, tRNA$^{Ala\text{-}UGC}$ is found in relatively low abundance, whereas tRNA$^{Gln\text{-}CUG}$ belongs to the group of highly abundant tRNAs (A.C. and Z.I., unpublished data). Hence, the increased level of uncharged tRNA$^{Gln\text{-}CUG}$ could not ameliorate the frameshifting

(D) Immunoblot analysis with HA antibodies of N2a/Htt103Q-CFP cells expressing Htt51Q(−1)YFP for 24 hr after separation by 1D SDS (left panel) and 2D gel electrophoresis (right panel). Note that the HA antibodies recognize both nonframeshifted Htt51Q (marked with *) and frameshifted Htt51Q-YFP (marked with #) proteins. MW, molecular weight.

(E) MALDI-TOF-MS analysis of N2a/Htt103Q-CFP cells expressing Htt51(−1)YFP for 24 hr.

See also Figure S1.

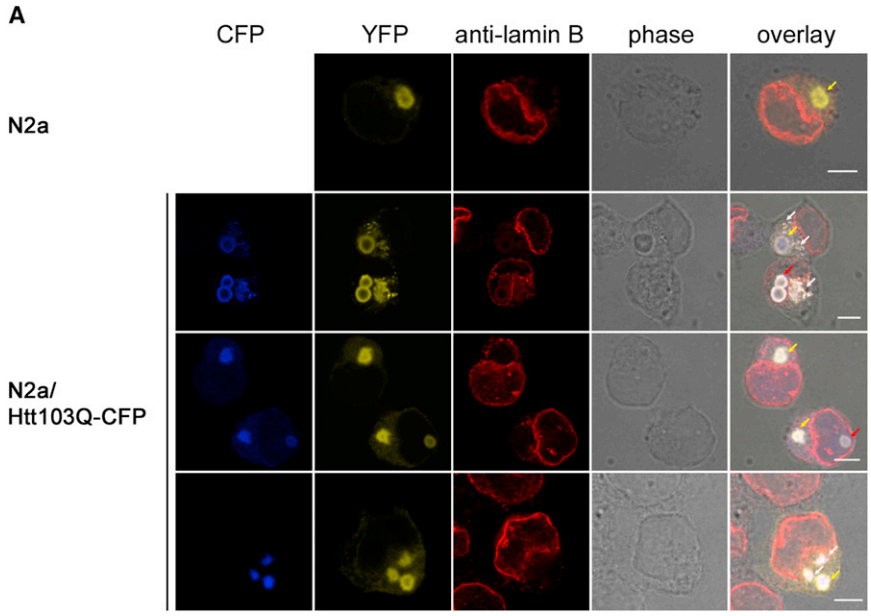

Figure 3. Frameshifted Proteins Form Inclusions with Different Morphologies in Neuronal N2a Cells

(A) Confocal fluorescent images of N2a and N2a/Htt103Q-CFP transfected with the Htt51Q(−1)YFP reporter and visualized after 24 hr by fluorescence (CFP and YFP) and phase contrast (phase) microscopy. The nuclear envelope was counterstained with lamin B antibody and Alexa-568-labeled secondary antibody (red channel). YFP-positive species localized in the nucleus are marked with a red arrow on the overlay image. The two morphologically distinct cytoplasmic inclusions (i.e., ring-shaped and solid hyperfluorescent puncta) are marked on the overlay images with yellow and white arrows, respectively. Scale bar, 5 μm.

(B) Confocal live-cell imaging of N2a/Htt103Q-CFP transfected with the Htt51Q(−1)YFP reporter. Time zero is the time after transfection of the reporter. Scale bar, 5 μm.

(C) N2a/Htt103Q-CFP cells expressing Htt51Q (−1)YFP were stained with LysoTrackerRED 24 hr after transfection. Scale bar, 5 μm.

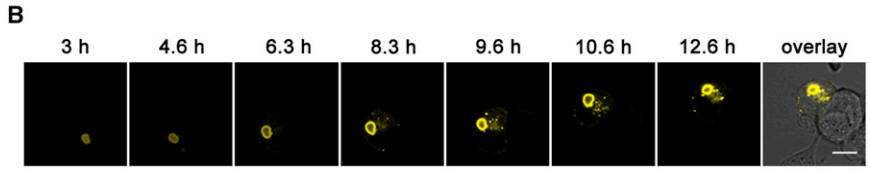

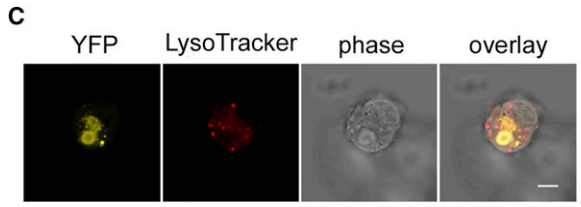

within the repetitive CAG stretches. Together, these results strongly support the hypothesis that −1 frameshifting within the CAG stretch is triggered by the depletion of the glutaminyl-tRNA$^{Gln\text{-}CUG}$ pool as a result of increased demand for this charged tRNA when translating proteins with homopolymeric CAG expansions.

Unexpectedly, when we compared the total amounts of tRNA$^{Gln\text{-}CUG}$ in nontransfected N2a and HeLa cells, we observed a lower concentration of tRNA$^{Gln\text{-}CUG}$ in N2a cells than in HeLa cells (Figure 2C), which provides an explanation for the observed higher frameshifting frequency in N2a cells (Figure 1C) than in HeLa cells (Figure S1A). This observation raised an intriguing question as to whether tRNA$^{Gln\text{-}CUG}$ levels vary among different brain tissues, which could contribute to the cell-selective pathology of HD. The most prominent early effects in HD have been observed in the striatum, even though striatal neurons do not selectively express higher levels of Htt mRNA (Landwehrmeyer et al., 1995). To address this issue, we used northern blotting to determine the total tRNA$^{Gln\text{-}CUG}$ concentration in four brain areas of 8-week-old mice. Intriguingly, the total amount of tRNA$^{Gln\text{-}CUG}$ was lower in the hippocampal and striatal homogenates compared with the cortex and cerebellum (Figure 2D).

Frameshifted Proteins Form Morphologically Distinct Aggregates In Vivo Dependent on the Q:A Ratio

To determine whether frameshifted HttQ/A proteins interact with nonframeshifted HttQ proteins and thus modulate their aggregation, we first analyzed the inclusions by confocal fluorescence microscopy. The majority of the YFP-positive inclusions formed ring-shaped structures surrounding the core aggregates composed of Htt103Q-CFP (Figure 3A). In addition, although less frequently, some cells contained smaller, dense hyperfluorescent puncta (Figure 3A). These two types of inclusion morphologies arose independently of each other, on different timescales (Figure 3B). The ring-shaped structures formed earlier, whereas the small, dense puncta appeared at later time points in the vicinity of the ring inclusions but did not fuse with them. The disperse punctal inclusions did not result from the autophagy-mediated clearance, because they did not colocalize with acidified compartments stained with LysoTracker (Figure 3C). Interestingly, regardless of their morphology, the inclusions that were composed of frameshifted species were frequently located in the vicinity of cytoplasmic or nuclear membranes. Some cytoplasmic aggregates in juxtanuclear positions formed local indentations in the nuclear membrane, and immunostaining revealed partly discontinuous

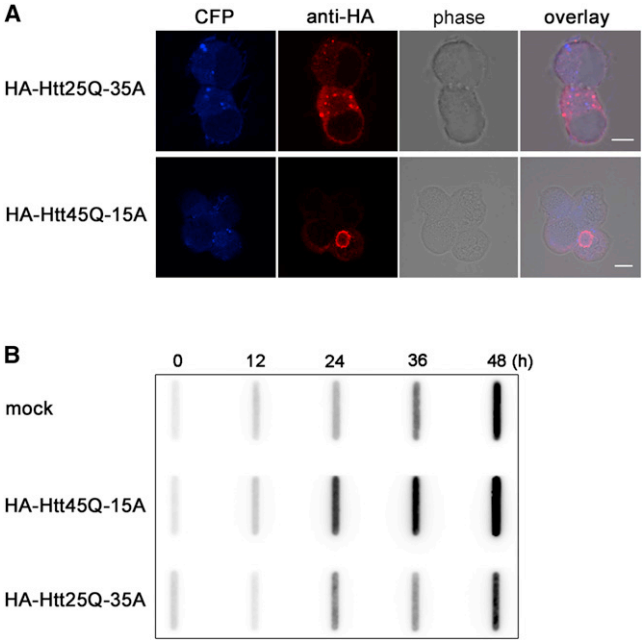

Figure 4. Frameshifted HttQ/A Proteins Modulate the Aggregation of Mutant Htt Exon 1 in a Q:A-Dependent Manner

(A) Confocal images of N2a/Htt103Q-CFP cells expressing HA-tagged Htt45Q-15A or Htt25Q-35A proteins and visualized after 24 hr by fluorescence (CFP, anti-HA) and phase contrast (phase) microscopy. The expression of Htt103Q-CFP was monitored by fluorescence (CFP), and HttQ/A proteins were detected by immunostaining of their N-terminal HA-tag 24 hr after transfection. Scale bar, 5 μm.

(B) Filter-retardation analysis of HeLa/Htt103Q-CFP cotransfected with Htt45Q-15A, Htt25Q-35A, or empty vector (mock) and immunostained with GFP antibodies recognizing Htt103Q-CFP aggregates. HttQ103-CFP expression was suppressed prior to transfection with doxacycline, so that it starts at zero. Because of the stable expression of Htt103Q-CFP, a small amount of SDS-resistant Htt103Q-CFP aggregates was detectable at 0 hr. See also Figure S3.

lamin B1 rims indicative of an altered nuclear envelope (Figure 3A).

Because Glu and Ala side chains have different physicochemical properties, we hypothesized that variations in the Q:A ratio in HttQ/A proteins, arising from the stochastic position of frameshifting within the CAG stretch, might explain the observed differences in the aggregate morphology. To test this hypothesis, we produced two stable HttQ/A proteins with a longer polyQ (Htt45Q-15A) and a longer polyA repeat (Htt25Q-35A), and compared them with the aggregate structures in N2a/Htt103Q-CFP and HeLa/Htt103Q-CFP cells (Figures 4A and S3). These hybrid proteins resembled the two dominant types of aggregate morphology that we observed in Htt51Q-YFP, i.e., Htt45Q-15A exclusively assembled into ring-shaped inclusions and Htt25Q-35A aggregated into dense hyperfluorescent puncta (Figures 4A and S3).

Next, we examined the effect of the hybrid proteins on the aggregation kinetics using a filter-retardation assay (Scherzinger et al., 1999) that retains only detergent-resistant prefibrillar and fibrillar aggregates (Kazantsev et al., 1999). The HttQ/A proteins influenced HttQ aggregation in a Q:A-dependent manner: Htt45Q-15A enhanced and Htt25Q-35A reduced the amount of sodium dodecyl sulfate (SDS)-resistant Htt103Q-CFP aggregates compared with the mock-transfected Htt103Q-CFP control cells (Figure 4B).

In Vitro Aggregation of HttQ/A Proteins

Intrigued by these in vivo effects, we next systematically analyzed the effects of frameshifted proteins on Htt52Q aggregation under defined in vitro conditions. We generated a library of Htt exon 1 variants with different Q:A ratios (Figure 5A), with a C-terminal region downstream of the polyQ/A stretch resembling the C terminus of our in vivo-generated frameshifted proteins (Figure 1A). Under physiological buffer conditions, the purified HttQ/A proteins (Figures S4A and S4B) rapidly assembled into amorphous aggregates with a morphology similar to the aggregates of polyalanine protein (Htt17A). They differed markedly, however, from the Htt52Q aggregates, which evolved from small spherical oligomers to SDS-resistant, electron-dense bundles of fibrils (Figures 5B and 5C). Interestingly, despite the lack of fibrillar morphology, the HttQ/A proteins formed SDS-resistant assemblies, although on a much slower timescale than Htt52Q, whereas the Htt17A aggregates remained SDS labile (Figure 5C). Among the constructs with a Q:A ratio > 1, the time course of formation of detergent-resistant aggregates correlated with the Q:A ratio, with SDS-resistant species forming most rapidly with Htt29Q-8A and most slowly with Htt20Q-15A (Figure 5C).

The two homopolymeric regions of the polyQ/A-hybrid stretch have different propensities for secondary structures. PolyQ peptides sample compact, collapsed, random coil structures when they are monomeric, and form β sheets in the aggregated state (Crick et al., 2006). Ala-rich peptides strongly favor an α-helical structure (Marqusee et al., 1989), although an expanded polyA peptide (>15) can also assemble into β-sheet complexes (Shinchuk et al., 2005). This raised the question as to whether HttQ/A proteins form a β-sheet-rich conformation on a much slower timescale than Htt52Q, which would explain the differences observed in the time course of formation of detergent-resistant aggregates. Circular dichroism (CD) spectroscopy under physiological conditions revealed that the monomeric HttQ/A proteins sampled a random coil conformation (Figure S4C) that was indistinguishable from the conformation of Htt52Q at the onset of aggregation (Figure S4D). At early aggregation time points, the CD spectra of the HttQ/A proteins showed a clear signature of an α-helical structure with negative bands at 208 nm and 222 nm, which were deeper for the constructs with longer polyA repeats (Figures 5D and S4E; Table S1). In the aggregation time course, the α-helicity of Htt29Q-8A and Htt15Q-15A progressively decreased in parallel with the enrichment of β-sheet-rich structural elements (Figure 5D; Table S1). Together, these results suggest that HttQ/A variants undergo a progressive conversion into β-sheet-rich aggregates, albeit on a much slower timescale compared with Htt52Q.

Hybrid HttQ/A Proteins Affect PolyQ Aggregation Kinetics in a Q:A-Dependent Manner

In vivo, we observed that frameshifted proteins affected the aggregation time course of HttQ proteins in different ways

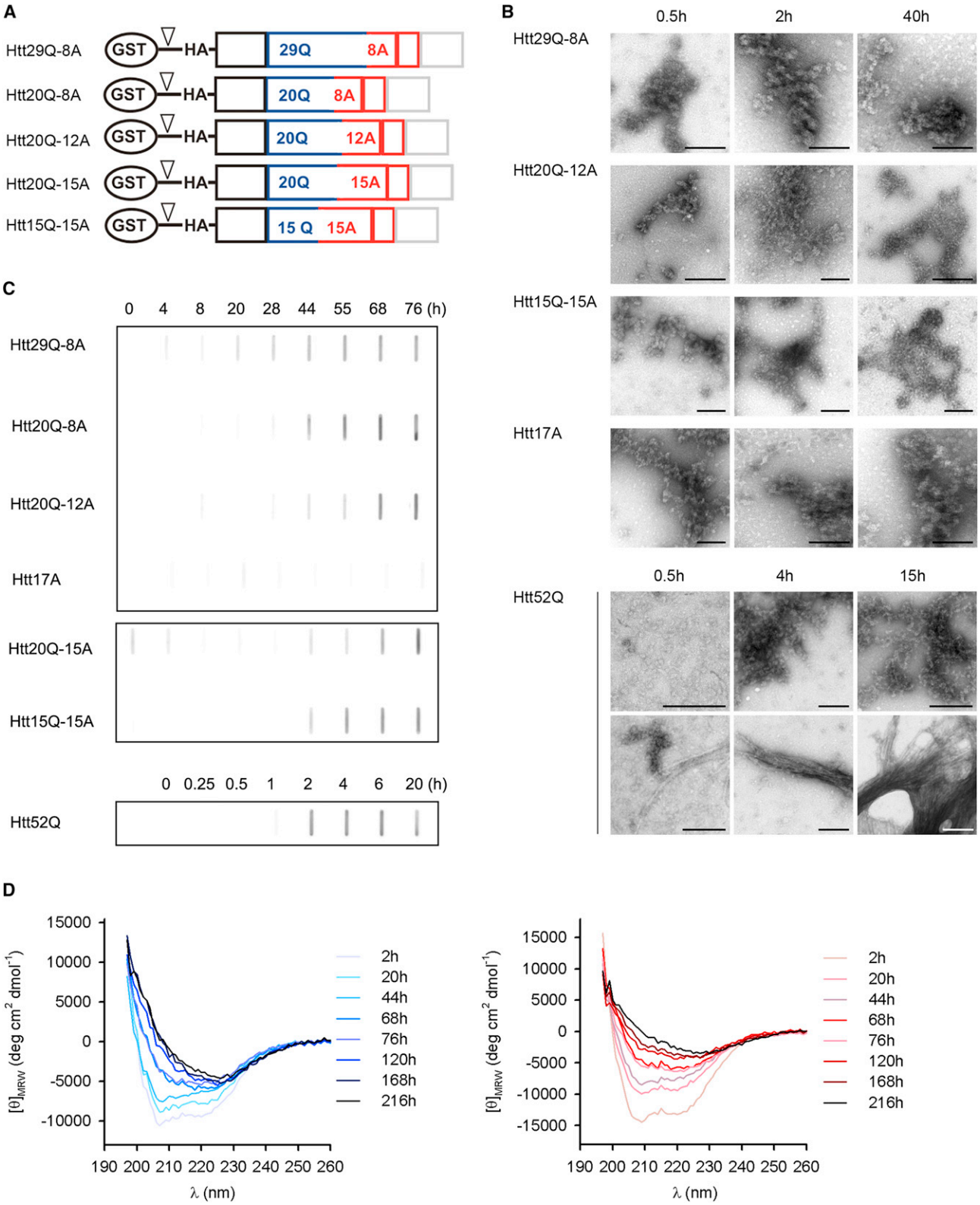

Figure 5. HttQ/A Proteins Form Detergent-Resistant Amorphous Aggregates In Vitro

(A) Schematic representation of the hybrid HttQ/A library. The HttQ/A proteins resemble the sequence of the frameshifted species in vivo and the color code is consistent with Figure 1A. The arrowhead indicates the PreScission protease cleavage site for removing the GST tag. All proteins have an N-terminal HA tag.

(legend continued on next page)

(Figures 3 and 4). To address this observation in more mechanistic detail, we analyzed the effect of monomer HttQ/A proteins on Htt52Q aggregation in vitro. Notably, the HttQ/A proteins exerted a clear Q:A-dependent effect on Htt52Q aggregation (Figure 6A). The two proteins with longer polyQ repeats (Htt29Q-8A and Htt20Q-8A) enhanced the Htt52Q aggregation, Htt20Q-12A had no influence, and hybrid constructs with longer polyA stretches (Htt20Q-15A and Htt15Q-15A) reduced the aggregation of Htt52Q (Figure 6A). When individually subjected to aggregation, the HttQ/A proteins did not scatter light at the concentration used in these experiments (Figure S5A). The HttQ/A proteins clearly coaggregated with Htt52Q. Immunogold labeling of Htt29Q-8A over its unique HA tag confirmed that Htt29Q-8A was integrated within the characteristic Htt52Q fibrils (Figure 6B) and that the aggregates were immunologically positive against antibodies that recognized Htt29Q-8A or Htt52Q (Figure S5C). In contrast, Ht17A, the protein with a homopolymeric A stretch, was not incorporated within the Htt52Q aggregates (Figure 6B), implying that the recruitment of HttQ/A proteins occurs through the polyQ stretch.

Recent studies proposed at least two phases in the aggregation time course of mutant Htt exon 1 (Tam et al., 2009; Thakur et al., 2009). Therefore, we next tested the effect of frameshifted HttQ/A proteins on the aggregation kinetics of Htt52Q. Intriguingly, an increase in the initial Htt29Q-8A concentration had a nonlinear effect on the kinetics of formation of detergent-resistant Htt52Q aggregates (Figure 6C). The lack of a proportional enhancement of the Htt52Q aggregation with an incremental increase of the HttQ/A monomer concentration implies that Htt29Q-8A might modulate various phases of the Htt52Q aggregation differently.

In a thioflavin T (ThT)-dye-binding assay, we resolved the two phases of Htt52Q aggregation (Figure 6D). The second phase coincided with the formation of SDS-resistant aggregates and most likely reflects the conversion of the initial oligomer species into fibrils (Figures 5B and 5C). We used this approach to perform a more detailed analysis of the effect of HttQ/A proteins with and without N-terminal 17 amino acids on Htt52Q aggregation. Deletion of the N17 domain of Htt20Q-8A (HttΔN20Q-8A) reduced Htt52Q aggregation compared with the full-length Htt20Q-8A protein (Figure 6E). The ThT-dye-binding assay showed that Htt20Q-8A enhanced Htt52Q aggregation by accelerating the first phase, increasing the aggregate yield. Interestingly, HttΔN20Q-8A slowed down the second phase of Htt52Q aggregation considerably without having an effect on the first phase (Figure 6D). The HttQ/A proteins were ThT-negative when they aggregated alone (Figure S5B); thus, any change in the ThT signal during the coaggregation reaction can be attributed to alterations in the Htt52Q aggregation. Together, these results indicate that the N17 domain and the polyA stretch exert a synergistic effect on Htt52Q oligomerization, and the polyA repeat modulates β-sheet nucleation depending on the Q:A proportions in the polyQ/A stretch.

DISCUSSION

Here, we analyze the frequency of frameshifting within the homopolymeric CAG repeat of Htt exon 1 and define the mechanisms by which frameshifted proteins modulate the aggregation of mutant Htt exon 1. Our data suggest that the high demand for charged $tRNA^{Gln\text{-}CUG}$ when reading expanded CAG repeats leads to a glutaminyl-$tRNA^{Gln\text{-}CUG}$ depletion, which shifts the reading frame predominantly in the −1 direction. The frequency of translational frameshifting strongly depends on the polyQ length. The kinetic rate constant for codon recognition measured in vitro is similar for all tRNAs, ~100 μM aminoacyl-$tRNA^{-1}s^{-1}$ (Gromadski et al., 2006), and is first order with respect to the concentration of tRNA, i.e., abundant tRNAs translate the cognate codon faster than low-abundance tRNAs (Zhang et al., 2009). In every round of the elongation cycle, new aminoacylated tRNA is delivered to the A site, whereas the former A-site tRNA is translocated to the ribosomal P site. Each tRNA is sequestered in the P site during the entire elongation cycle of the next upstream codon, and this time actually doubles when two consecutive codons of the same type are translated (Varenne and Lazdunski, 1986). Even though $tRNA^{Gln\text{-}CUG}$ is relatively abundant in eukaryotic cells (A.C. and Z.I., unpublished data), the simultaneous translation of several mRNA copies with consecutive CAG codons sequesters a large fraction of glutaminyl-$tRNA^{Gln\text{-}CUG}$ in the ribosomal P sites. This decreases the amount of free $tRNA^{Gln\text{-}CUG}$ that can be aminoacylated for a next translation round. In addition, tRNA aminoacylation, a rate-limiting process in eukaryotes (Zhang et al., 2010), also decreases the amount of free glutaminyl-$tRNA^{Gln\text{-}CUG}$, leaving many A sites vacant. Hungry A-site codons have been shown to significantly enhance the frequency of programmed frameshifting in bacteria (Liao et al., 2008; Lindsley et al., 2003) and yeast retrotransposons (Kawakami et al., 1993), but in the +1 frame rather than in the −1 frame. In general, programmed ribosomal frameshifting strongly depends on the propensity for slippage of P-site tRNA, which allows for repositioning in an alternative reading frame by vacant A sites (Baranov et al., 2004; Liao et al., 2008). This repositioning is possible in both directions (Baranov et al., 2004), but the tendency to reposition toward the −1 frame inversely correlates with the stability of codon–anticodon interactions in the E site (Sanders and Curran, 2007) and is enhanced by the presence of a stable secondary structure or a pseudoknot downstream of the A codon (Lindsley and Gallant, 1993; Wills et al., 2006). The CAG codon establishes a stable codon-anticodon interaction (Sanders and Curran, 2007) in the E site, which would favor less frameshifting. However, the strong propensity of CAG repeats within Htt exon 1 to form stable secondary structures (Michlewski and Krzyzosiak, 2004) in combination with vacant A sites explains the higher frequency of −1 frameshifting. We cannot exclude the possibility that depletion of glutaminyl-$tRNA^{Gln\text{-}CUG}$ might commonly occur when other expanded CAG-repeat disease proteins are

(B and C) Aggregation time course of HttQ/A (2 μM), Htt52Q (4 μM), and Htt17A (2 μM) at 30°C monitored by electron microscopy (B) and a filter-retardation assay with HA antibodies (C). Scale bar, 200 nm (B).
(D) Aggregation time course of Htt29Q-8A (3 μM; left plot) and Htt15Q-15A (3 μM; right plot) monitored by far-UV CD at 30°C.
See also Figure S4 and Table S1.

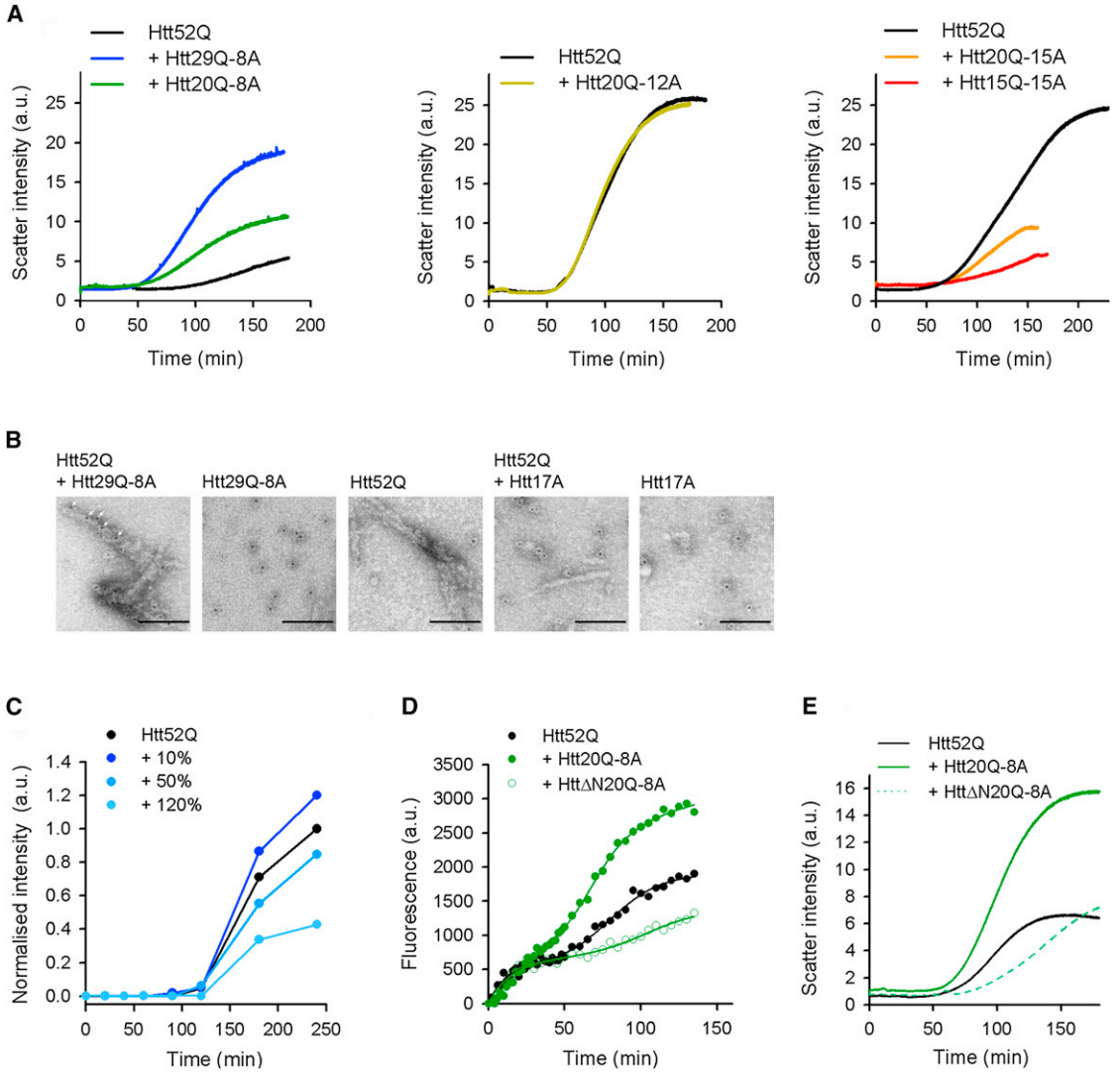

Figure 6. HttQ/A Proteins Modulate Htt52Q Aggregation Differently In Vitro

(A) Coaggregation of monomeric HttQ/A proteins (10%) added at the onset of Htt52Q aggregation and monitored by static light scattering at 90°C. Concentration of Htt52Q (from left to right): 2.8, 4, and 3.5 μM. The aggregation curve of Htt52Q alone is included in each plot as a control.

(B) Immunogold labeling of Htt52Q fibrils grown in the presence of 10% Htt29Q-8A or Htt17A. Incorporated Htt29Q-8A monomers in the Htt52Q fibrils are highlighted with white arrows. Gold-labeled antibody binds only to the HA tag of Htt29Q-8A and Htt17A. Aggregated Htt29Q-8A and Htt17A served as positive controls. Htt52Q, which lacks an HA tag, served as a negative control and is not gold-labeled. Scale bar: 200 nm.

(C) Various concentrations of Htt29Q-8A were added to Htt52Q at the start of aggregation and the SDS-resistant aggregates were detected by a filter-retardation assay with His antibody, which only recognizes the Htt52Q protein. The data are represented as normalized graphical plots (see Extended Experimental Procedures).

(D and E) Coaggregation of Htt52Q (4 μM) and 10% monomeric Htt20Q-8A or HttΔN20Q-8A monitored by ThT-binding assay (D) and light scattering at 90° (E). ThT curves were fitted to a two-phase kinetic model; all curve fits yielded $R^2 > 0.96$.

See also Figure S5.

expressed, but whether it results in frameshifting remains to be determined for each protein. It is important to note that the sequences flanking the CAG repeat strongly modulate its secondary structure stability (Michlewski and Krzyzosiak, 2004) and thus may result in large variations in the mechanism and propensity for frameshifting of different polyQ proteins.

Two putative slippery sequences, gaAAAG (encoding EK) and auGAAG (encoding MK; Figure 1A), were identified within the N17 region (Wills and Atkins, 2006). A translational −1 frameshift at one of these sites would be independent of the CAG-repeat length and would generate a single product in which the CAG-frame (polyQ) would be completely converted into a GCA-frame (polyA). Although we did not detect any proteins composed solely of polyA stretches, we cannot rule out a possible contribution of these two frameshift-stimulatory sequences to the frameshifting of HttQ in vivo. The frequency of this frameshifting event

may be too low to detect, given that −1 frameshifting at slippery sequences in mammalian in vitro systems occurs at a rate of ~2% (Brierley and Pennell, 2001).

The variations in the $tRNA^{Gln\text{-}CUG}$ concentration in different cell lines and mouse brain tissues support the notion that variations in the tRNA pool may represent a selective adaptation to match the biosynthetic demands and protein repertoires in various cells and tissues. However, on the level of translation, lower $tRNA^{Gln\text{-}CUG}$ concentrations would potentiate the impact of expanded CAG repeats expression. The steady-state concentration of endogenous Htt mRNA in brain tissues is not known, and because of instrumental sensitivity constraints, direct experimental determination of the frameshifting frequency of endogenous Htt is not possible. However, the presence of polyA or polyS proteins in HD-affected brain tissues (Davies and Rubinsztein, 2006) and the higher propensity for frameshifting in neurons (van Leeuwen et al., 1998) provide evidence that frameshifting may occur during translation of endogenous mutant Htt with an expanded CAG repeat in brain tissues. The striatum is an early target of HD, and one of the lowest $tRNA^{Gln\text{-}CUG}$ concentrations we measured in brain regions of mice was in the striatum. For these measurements we used homogenized brain areas containing terminally differentiated neurons and replicating progenitor populations, so the actual levels of $tRNA^{Gln\text{-}CUG}$ might be much higher in terminally differentiated cells. This suggests that frameshifting may occur with much higher frequency in the striatal neurons or at a much lower mRNA concentration of mutant Htt, i.e., at a much lower amount of total CAG codons expressed in one cell. Moreover, the mutant CAG repeat allele in the striatal neurons is highly unstable and is usually extended by >10 CAG codons compared with that in the progenitor allele or in other brain tissues (Gonitel et al., 2008; Kennedy et al., 2003). Thus, the lower $tRNA^{Gln\text{-}CUG}$ concentration together with the somatic CAG-repeat instability in the striatum may act as a significant disease modifier in HD.

The amphipathic N17 region in mutant Htt exon 1 associates in helical bundles through its nonpolar interfaces (Tam et al., 2009), thereby increasing the local concentration of the polyQ monomers and facilitating β-sheet nucleation and fibrillization (Thakur et al., 2009). Additionally, the high α-helical propensity of the polyA stretch most likely facilitates the initial association of Htt monomers in these bundled structures, which is consistent with the observed acceleration of the first phase of Htt52Q aggregation (Figure 6D). The helical structures can be also stabilized by membrane surfaces: in-cell aggregates containing frameshifted species preferably localize at the nuclear or plasma membrane (Figure 3). Helix-mediated association plays a central role in the amyloidogenesis of some other proteins and peptides (Abedini and Raleigh, 2009; Williamson et al., 2009), increasing the local concentration of fibrillization-prone monomers to nucleate intermolecular β-sheet formation (Abedini and Raleigh, 2009). It is important to note that this model cannot be transferred to all CAG-frameshifted species, because that would imply that a polyA length increase in HttQ/A proteins should proportionally enhance HttQ fibrillization. Instead, the Q:A-ratio-dependent effect on Htt52Q aggregation (Figure 6A) supports the notion that crosstalk between polyA and N17 modulate HttQ fibrillization. Shorter polyA stretches, resulting from frameshifting later in the CAG repeat, do not impair the nucleation of β-strand structures even within the hybrid polyQ/A stretches. In contrast, frameshifted HttQ/A species with longer polyA repeats, which form SDS-resistant species on a much slower timescale, most likely decrease β-sheet nucleation by reducing the concentration of the fibrillization-competent monomers in the initial aggregates. The time-dependent variations of polyQ aggregation in the presence of different HttQ/A proteins and the sensitivity of the HttQ/A conformations to small changes in the primary structure (i.e., in the Q:A ratio) are reminiscent of the prion model, in which changes in the self-perpetuating prionic conformation alter the strain phenotypes and specificity of propagation (Chien et al., 2004).

The crystal structure of a fusion protein of maltose-binding protein and Htt17Q (Kim et al., 2009), and structural studies on thioredoxin fusion to polyQ peptides (Nagai et al., 2007) suggest that the polyQ domain populates an α-helical conformation. α-Helical structures may represent on-pathway intermediate structures of the monomeric polyQ proteins that facilitate the conversion of coiled-coil fibers into β-sheet polymers (Fiumara et al., 2010). Our results do not exclude the possibility that the polyA repeat may interfere with the transition to a β-sheet structure by stabilizing the polyQ domain in an α-helical conformation. If such a helical conformation were populated, the effect should be strongly dependent on the Q:A ratio and might apply to a frameshifting event close to the 5′-terminus of the CAG-repeat, which generates HttQ/A proteins with Q:A < 1.

In summary, our analysis of the translation fidelity of CAG repeats reveals that translation of long, consecutive homopolymeric stretches is a challenge for the translation machinery and causes an imbalance in the stoichiometry between charged, cognate $tRNA^{Gln\text{-}CUG}$ and CAG codons to be translated. The shortage of the glutaminyl-$tRNA^{Gln\text{-}CUG}$ leads to a −1 frameshifting within the CAG repeat. Every codon in the CAG repeat is equally susceptible to frameshifting, and various polyQ/A proteins can be generated within a tissue or a cell. Depending on the Q:A ratio, the HttQ/A hybrid proteins modulate the conformational switch differently to nucleate HttQ fibrillization and thus contribute to the heterogeneity of the aggregation process. In conclusion, these results add to the emerging concept that, beyond polypeptide folding, alterations in the homeostasis of various cellular processes (here translation) have important implications for the neurodegenerative pathologies. Our findings suggest that frameshifting within the expanded CAG stretches, which is stochastic in its nature, may act as a disease modifier and may contribute to the heterogeneity in disease course and onset on both cellular and individual levels.

EXPERIMENTAL PROCEDURES

Cell Culture, Imaging, and tRNA

N2a and HeLa cells stably transfected with Htt25Q-CFP, Htt65Q-CFP, or Htt103Q-CFP were a kind gift from Dr. Ai Yamamoto and were cultured as previously described (Yamamoto et al., 2006). Htt51Q(−1)YFP was cloned into pTRE2hyg Tet-off plasmid and transfected using JetPrime reagent in N2a (PeqLab) or Lipofectamine in HeLa cells (Invitrogen). For siRNA experiments in the N2a cells, Htt51Q(−1)YFP was cotransfected with pSuper

plasmid (1:1 ratio, 1 μg DNA in total) bearing small hairpin RNA (shRNA) targeting $tRNA^{Gln\text{-}CUG}$ or $tRNA^{Thr\text{-}AGU}$. The levels of intrinsic $tRNA^{Gln\text{-}CUG}$, $tRNA^{Thr\text{-}AGU}$, or $tRNA^{Ala\text{-}UGC}$ were raised according to a previously described procedure (Geslain and Pan, 2010).

The HA-tagged Htt51Q(−1)YFP was immunostained with monoclonal HA.11 antibody (Covance) and Alexa-568-labeled anti-mouse secondary antibody (Invitrogen). To monitor the acidified compartments, cells were incubated with 75 nM LysoTrackerRED (Invitrogen). Cells were imaged on an LSM710 Axiovert confocal microscope (Zeiss) at laser wavelengths of 405 nm for CFP, 514 nm for YFP, and 561 nm for Alexa568-labeled antibodies or LisoTrackerRED.

tRNA Extraction and Analysis

The striatum, cortex, cerebellum, and hippocampus were separated from the whole brains of three C57B16 mice and each was homogenized in 2 ml TriReagent (Sigma). The experiments with mice were approved by the Animal Experiment Committee of Brandenburg. Total deacylated tRNA from cells and brain tissues was directly isolated from the TriReagent-treated homogenates, and the total aminoacyl-tRNA was extracted from cells with acidic phenol (pH 4.5) as previously described (Varshney et al., 1991). $tRNA^{Gln\text{-}CUG}$ in brain and cell homogenates was detected by northern blot with Cy3-labeled 14-mer oligonucleotide complementary to the anticodon loop or ^{33}P-labeled oligonucleotide pairing to the full-length $tRNA^{Gln\text{-}CUG}$. Statistical analyses were performed with Fisher's exact test and permutation test. Differences were considered statistically significant when $p < 0.05$.

Immunoblotting and MS

A total of 250,000 cells were directly harvested in 200 μl formic acid, incubated at 37°C for 2 hr to dissolve aggregates, resolved by one-dimensional (1D) or two-dimensional (2D) gel electrophoresis, and detected by immunostaining with HA.11 antibodies.

For MS, cell lysates were immunoprecipitated with green fluorescent protein (GFP) antibodies (MicroBeads; Miltenyi) and separated by 2D gel electrophoresis. Protein spots were excised and digested with 30 ng/μl trypsin (sequencing grade; Roche) at 37°C for 12 hr, dephosphorylated with Antarctic phosphatase for 30 min, and analyzed by MALDI-TOF-MS (microflex LRF; Bruker Daltonics) in linear mode.

In Vitro Aggregation Assays

Proteins were expressed as glutathione S-transferase (GST) fusions on the pGEX-6P-1 plasmid (GE Healthcare) in *Escherichia coli* BL21(DE3) and affinity purified with glutathione-sepharose 4 fast flow (GE Healthcare) as previously described (Scherzinger et al., 1999). Aggregation was initiated by addition of PreScission protease, which removes the GST tag, and monitored by means of a filter-retardation assay (Scherzinger et al., 1999), ThT analysis (Lee et al., 2011), static 90° light scattering at 532 nm (Quanta Master 30; PTI), and far-UV CD spectroscopy (Jasco-815).

Electron Microscopy and Immunogold Labeling

For electron microscopy, 20 μl aliquots were withdrawn from an ongoing in vitro aggregation reaction and spotted onto glow-discharged, carbon-coated 400 mesh copper grids, stained with 1% uranyl acetate, and imaged on an 80 kV (CEM 902; Zeiss) or 120 kV (G2 Spirit; Tecnai) transmission electron microscope.

For immunogold labeling, overnight aggregated samples were absorbed onto the copper grids, labeled with HA.11 monoclonal antibody and gold-conjugated secondary mouse antibody (Britisch Biocell International), stained for 2 min in 0.5% uranyl acetate, and imaged on an 80 kV transmission electron microscope (CEM 902; Zeiss).

For further details, see the Extended Experimental Procedures.

SUPPLEMENTAL INFORMATION

Supplemental Information includes five figures, one table, and Extended Experimental Procedures and can be found with this article online at http://dx.doi.org/10.1016/j.celrep.2012.12.019.

LICENSING INFORMATION

ACKNOWLEDGMENTS

We are grateful to Ai Yamamoto (Columbia University) for the N2a/HttQ-CFP and HeLa/HttQ-CFP cells, Rolf Heumann and Daniela Damen (Ruhr University of Bochum) for providing the mouse brain tissues, Marcel Naumann and Klaus Gast (University of Potsdam) for support with the CD spectroscopy, Kajetan Bentele (Humboldt University of Berlin) for help with the statistical analysis, and Otto Baumann and Jörg Fettke (University of Potsdam) for help with the confocal microscope and MS analysis. This work was supported by grants from the DFG (IG 73/10-1 and SFB 740 [A5]) to Z.I. and a DOC fFORTE fellowship from the Austrian Academy of Sciences to H.G.

Received: June 17, 2012
Revised: October 17, 2012
Accepted: December 28, 2012
Published: January 24, 2013

REFERENCES

Abedini, A., and Raleigh, D.P. (2009). A critical assessment of the role of helical intermediates in amyloid formation by natively unfolded proteins and polypeptides. Protein Eng. Des. Sel. *22*, 453–459.

Amiel, J., Trochet, D., Clément-Ziza, M., Munnich, A., and Lyonnet, S. (2004). Polyalanine expansions in human. Hum. Mol. Genet. *13*(Spec No 2), R235–R243.

Andresen, J.M., Gayán, J., Djoussé, L., Roberts, S., Brocklebank, D., Cherny, S.S., Cardon, L.R., Gusella, J.F., MacDonald, M.E., Myers, R.H., et al.; US-Venezuela Collaborative Research Group; HD MAPS Collaborative Research Group. (2007). The relationship between CAG repeat length and age of onset differs for Huntington's disease patients with juvenile onset or adult onset. Ann. Hum. Genet. *71*, 295–301.

Atkins, J.F., Gesteland, R.F., Reid, B.R., and Anderson, C.W. (1979). Normal tRNAs promote ribosomal frameshifting. Cell *18*, 1119–1131.

Baranov, P.V., Gesteland, R.F., and Atkins, J.F. (2004). P-site tRNA is a crucial initiator of ribosomal frameshifting. RNA *10*, 221–230.

Brierley, I., and Pennell, S. (2001). Structure and function of the stimulatory RNAs involved in programmed eukaryotic-1 ribosomal frameshifting. Cold Spring Harb. Symp. Quant. Biol. *66*, 233–248.

Brinkman, R.R., Mezei, M.M., Theilmann, J., Almqvist, E., and Hayden, M.R. (1997). The likelihood of being affected with Huntington disease by a particular age, for a specific CAG size. Am. J. Hum. Genet. *60*, 1202–1210.

Chien, P., Weissman, J.S., and DePace, A.H. (2004). Emerging principles of conformation-based prion inheritance. Annu. Rev. Biochem. *73*, 617–656.

Crick, S.L., Jayaraman, M., Frieden, C., Wetzel, R., and Pappu, R.V. (2006). Fluorescence correlation spectroscopy shows that monomeric polyglutamine molecules form collapsed structures in aqueous solutions. Proc. Natl. Acad. Sci. USA *103*, 16764–16769.

Davies, J.E., and Rubinsztein, D.C. (2006). Polyalanine and polyserine frameshift products in Huntington's disease. J. Med. Genet. *43*, 893–896.

Fiumara, F., Fioriti, L., Kandel, E.R., and Hendrickson, W.A. (2010). Essential role of coiled coils for aggregation and activity of Q/N-rich prions and PolyQ proteins. Cell *143*, 1121–1135.

Geslain, R., and Pan, T. (2010). Functional analysis of human tRNA isodecoders. J. Mol. Biol. *396*, 821–831.

Gidalevitz, T., Ben-Zvi, A., Ho, K.H., Brignull, H.R., and Morimoto, R.I. (2006). Progressive disruption of cellular protein folding in models of polyglutamine diseases. Science *311*, 1471–1474.

Gonitel, R., Moffitt, H., Sathasivam, K., Woodman, B., Detloff, P.J., Faull, R.L., and Bates, G.P. (2008). DNA instability in postmitotic neurons. Proc. Natl. Acad. Sci. USA *105*, 3467–3472.

Gromadski, K.B., Daviter, T., and Rodnina, M.V. (2006). A uniform response to mismatches in codon-anticodon complexes ensures ribosomal fidelity. Mol. Cell *21*, 369–377.

Kawakami, K., Pande, S., Faiola, B., Moore, D.P., Boeke, J.D., Farabaugh, P.J., Strathern, J.N., Nakamura, Y., and Garfinkel, D.J. (1993). A rare tRNA-Arg(CCU) that regulates Ty1 element ribosomal frameshifting is essential for Ty1 retrotransposition in Saccharomyces cerevisiae. Genetics *135*, 309–320.

Kazantsev, A., Preisinger, E., Dranovsky, A., Goldgaber, D., and Housman, D. (1999). Insoluble detergent-resistant aggregates form between pathological and nonpathological lengths of polyglutamine in mammalian cells. Proc. Natl. Acad. Sci. USA *96*, 11404–11409.

Kennedy, L., Evans, E., Chen, C.M., Craven, L., Detloff, P.J., Ennis, M., and Shelbourne, P.F. (2003). Dramatic tissue-specific mutation length increases are an early molecular event in Huntington disease pathogenesis. Hum. Mol. Genet. *12*, 3359–3367.

Kim, M.W., Chelliah, Y., Kim, S.W., Otwinowski, Z., and Bezprozvanny, I. (2009). Secondary structure of Huntingtin amino-terminal region. Structure *17*, 1205–1212.

Landwehrmeyer, G.B., McNeil, S.M., Dure, L.S., 4th, Ge, P., Aizawa, H., Huang, Q., Ambrose, C.M., Duyao, M.P., Bird, E.D., Bonilla, E., et al. (1995). Huntington's disease gene: regional and cellular expression in brain of normal and affected individuals. Ann. Neurol. *37*, 218–230.

Lee, J., Culyba, E.K., Powers, E.T., and Kelly, J.W. (2011). Amyloid-β forms fibrils by nucleated conformational conversion of oligomers. Nat. Chem. Biol. *7*, 602–609.

Liao, P.Y., Gupta, P., Petrov, A.N., Dinman, J.D., and Lee, K.H. (2008). A new kinetic model reveals the synergistic effect of E-, P- and A-sites on +1 ribosomal frameshifting. Nucleic Acids Res. *36*, 2619–2629.

Lindsley, D., and Gallant, J. (1993). On the directional specificity of ribosome frameshifting at a "hungry" codon. Proc. Natl. Acad. Sci. USA *90*, 5469–5473.

Lindsley, D., Gallant, J., and Guarneros, G. (2003). Ribosome bypassing elicited by tRNA depletion. Mol. Microbiol. *48*, 1267–1274.

Marqusee, S., Robbins, V.H., and Baldwin, R.L. (1989). Unusually stable helix formation in short alanine-based peptides. Proc. Natl. Acad. Sci. USA *86*, 5286–5290.

Michlewski, G., and Krzyzosiak, W.J. (2004). Molecular architecture of CAG repeats in human disease related transcripts. J. Mol. Biol. *340*, 665–679.

Nagai, Y., Inui, T., Popiel, H.A., Fujikake, N., Hasegawa, K., Urade, Y., Goto, Y., Naiki, H., and Toda, T. (2007). A toxic monomeric conformer of the polyglutamine protein. Nat. Struct. Mol. Biol. *14*, 332–340.

Orr, H.T., and Zoghbi, H.Y. (2007). Trinucleotide repeat disorders. Annu. Rev. Neurosci. *30*, 575–621.

Sanders, C.L., and Curran, J.F. (2007). Genetic analysis of the E site during RF2 programmed frameshifting. RNA *13*, 1483–1491.

Scherzinger, E., Sittler, A., Schweiger, K., Heiser, V., Lurz, R., Hasenbank, R., Bates, G.P., Lehrach, H., and Wanker, E.E. (1999). Self-assembly of polyglutamine-containing huntingtin fragments into amyloid-like fibrils: implications for Huntington's disease pathology. Proc. Natl. Acad. Sci. USA *96*, 4604–4609.

Shinchuk, L.M., Sharma, D., Blondelle, S.E., Reixach, N., Inouye, H., and Kirschner, D.A. (2005). Poly-(L-alanine) expansions form core beta-sheets that nucleate amyloid assembly. Proteins *61*, 579–589.

Tam, S., Spiess, C., Auyeung, W., Joachimiak, L., Chen, B., Poirier, M.A., and Frydman, J. (2009). The chaperonin TRiC blocks a huntingtin sequence element that promotes the conformational switch to aggregation. Nat. Struct. Mol. Biol. *16*, 1279–1285.

Thakur, A.K., Jayaraman, M., Mishra, R., Thakur, M., Chellgren, V.M., Byeon, I.J., Anjum, D.H., Kodali, R., Creamer, T.P., Conway, J.F., et al. (2009). Polyglutamine disruption of the huntingtin exon 1 N terminus triggers a complex aggregation mechanism. Nat. Struct. Mol. Biol. *16*, 380–389.

Toneff, T., Mende-Mueller, L., Wu, Y., Hwang, S.R., Bundey, R., Thompson, L.M., Chesselet, M.F., and Hook, V. (2002). Comparison of huntingtin proteolytic fragments in human lymphoblast cell lines and human brain. J. Neurochem. *82*, 84–92.

Toulouse, A., Au-Yeung, F., Gaspar, C., Roussel, J., Dion, P., and Rouleau, G.A. (2005). Ribosomal frameshifting on MJD-1 transcripts with long CAG tracts. Hum. Mol. Genet. *14*, 2649–2660.

van Leeuwen, F.W., de Kleijn, D.P., van den Hurk, H.H., Neubauer, A., Sonnemans, M.A., Sluijs, J.A., Köycü, S., Ramdjielal, R.D., Salehi, A., Martens, G.J., et al. (1998). Frameshift mutants of beta amyloid precursor protein and ubiquitin-B in Alzheimer's and Down patients. Science *279*, 242–247.

Varenne, S., and Lazdunski, C. (1986). Effect of distribution of unfavourable codons on the maximum rate of gene expression by an heterologous organism. J. Theor. Biol. *120*, 99–110.

Varshney, U., Lee, C.P., and RajBhandary, U.L. (1991). Direct analysis of aminoacylation levels of tRNAs in vivo. Application to studying recognition of Escherichia coli initiator tRNA mutants by glutaminyl-tRNA synthetase. J. Biol. Chem. *266*, 24712–24718.

Williamson, J.A., Loria, J.P., and Miranker, A.D. (2009). Helix stabilization precedes aqueous and bilayer-catalyzed fiber formation in islet amyloid polypeptide. J. Mol. Biol. *393*, 383–396.

Wills, N.M., and Atkins, J.F. (2006). The potential role of ribosomal frameshifting in generating aberrant proteins implicated in neurodegenerative diseases. RNA *12*, 1149–1153.

Wills, N.M., Moore, B., Hammer, A., Gesteland, R.F., and Atkins, J.F. (2006). A functional -1 ribosomal frameshift signal in the human paraneoplastic Ma3 gene. J. Biol. Chem. *281*, 7082–7088.

Yamamoto, A., Cremona, M.L., and Rothman, J.E. (2006). Autophagy-mediated clearance of huntingtin aggregates triggered by the insulin-signaling pathway. J. Cell Biol. *172*, 719–731.

Zhang, G., Hubalewska, M., and Ignatova, Z. (2009). Transient ribosomal attenuation coordinates protein synthesis and co-translational folding. Nat. Struct. Mol. Biol. *16*, 274–280.

Zhang, G., Fedyunin, I., Miekley, O., Valleriani, A., Moura, A., and Ignatova, Z. (2010). Global and local depletion of ternary complex limits translational elongation. Nucleic Acids Res. *38*, 4778–4787.

Zu, T., Gibbens, B., Doty, N.S., Gomes-Pereira, M., Huguet, A., Stone, M.D., Margolis, J., Peterson, M., Markowski, T.W., Ingram, M.A., et al. (2011). Non-ATG-initiated translation directed by microsatellite expansions. Proc. Natl. Acad. Sci. USA *108*, 260–265.